IEEE Access
Multidisciplinary | Rapid Review | Open Access Journal

Received 10 March 2024, accepted 9 April 2024, date of publication 16 April 2024, date of current version 23 April 2024.

Digital Object Identifier 10.1109/ACCESS.2024.3388491

RESEARCH ARTICLE

Fuzzy Logic Controlled Pulse Density Modulation Technique for Bidirectional Inductive Power Transfer Systems

MURUGAN VENKATESAN[1], R. NARAYANAMOORTHI[1], AHMED EMARA[2,3], AND YAZEED YASIN GHADI[4]

[1]Department of Electrical and Electronics Engineering, Wireless Charging Research Centre, SRM Institute of Science and Technology, Kattankulathur, Chennai 603203, India
[2]Electrical Engineering Department, University of Business and Technology, Ar Rawdah, Jeddah 23435, Saudi Arabia
[3]Engineering Mathematics and Physics Department, Faculty of Engineering, Alexandria University, Alexandria 21544, Egypt
[4]Department of Computer Science and Software Engineering, Al Ain University, Abu Dhabi, United Arab Emirates

Corresponding authors: R. Narayanamoorthi (narayanamoorthi.r@gmail.com) and Ahmed Emara (a.emara@ubt.edu.sa)

This work was supported in part by the Government of India, Department of Science and Technology (DST), Science and Engineering Research Board (SERB) Core Research, under Grant CRG/2020/004073.

ABSTRACT The human intervention free bidirectional efficient energy exchange between the grid and Electric Vehicles (EVs) relies on effective bidirectional power flow control in Wireless Power Transfer (WPT) system. This essential bidirectional control feature enables the grid to charge the EV's battery and, during surplus energy periods, allows the EV to feed power back to the grid. This capability facilitates the implementation of Vehicle-to-Grid (V2G) functionalities. Implementing this bidirectional flow requires sophisticated modulation techniques to ensure seamless power transfer and optimize overall efficiency. In comparison to pulse width modulation, pulse density modulation (PDM) proves more effective in minimizing switching losses in the converter. PDM efficiently manages the amplitude of high-frequency pulses generated by the inverter and converter systems for WPT applications. However, the PDM techniques are not effectively investigated in the bidirectional wireless power transfer system (BWPT). In this paper, Fuzzy Logic Controlled Pulse Density Modulation (FLC-PDM) approach for the BWPT is proposed for the first time. This approach uses dual side pulse density control for high-frequency converters with the fuzzy rule base to adjust the pulse density and duty ratio based on the load demand. The proposed approach aiming to optimize efficiency across diverse loads and regulate the output voltage and provides effective control approach for the BWPT system. This method ensures constant switching frequency output voltage regulation and delicate shifting operation for high-frequency converter switches, requiring no additional components. The circuit simulations and hardware prototype testing are performed for the 3.7 kW power rating and 85 kHz operating frequency to validate the proposed FLC-PDM approach for the BWPT circuit and yielded an efficiency over 93% across diverse load resistances and pulse densities.

INDEX TERMS Electric vehicle (EV), bidirectional inductive power transfer (BIPT), pulse width modulation (PWM), pulse density modulation (PDM), zero-current switching (ZCS), zero-voltage switching (ZVS).

I. INTRODUCTION

Frequent power outages, escalating due to an aging grid and climate change, have led to economic costs of $100-$200 billion annually, impacting comfort, productivity, and public safety [1], [2]. Distribution system outages are more common than transmission system disruptions which requires effective solutions [3], [4]. The growing interest in EVs introduces the potential requirement for mobile Energy Storage Systems (ESSs) to serve as backup power sources, spinning/non-spinning reserves, and grid regulation providers [5], [6]. Despite their marketability, current EVs lack the capability

The associate editor coordinating the review of this manuscript and approving it for publication was Tariq Masood.

to share the power to the power grid or provide services, attributed to unidirectional charging systems. Integrating EVs into the energy landscape shows promise for supporting renewable energy and stationary ESS, enhancing grid resilience and stability. Overcoming charging limitations in EVs represents a crucial step towards realizing their full potential in grid services and emergency backup power [7]. WPT through inductive coupling has emerged as a versatile technology, facilitating the wireless transmission of electrical energy between sources and loads [8]. This approach ensures flexibility, precision, and safety, proving effective in industrial and everyday applications. Current research focuses on achieving low cost, simplicity, and reliability, particularly in the context of charging EVs [9]. The rise of bidirectional WPT systems, particularly for EV charging, underscores the significance of a time-varying magnetic field in inducing voltage for effective bidirectional power transfer [10]. Traditionally, WPT systems focused on one-way power flow, with research aimed at improving efficiency, compensation strategies, and handling misalignment. However, recent applications demand bi-directional power flow, such as those involving regenerative braking, vehicle-to-grid (V2G), or vehicle-to-home (V2H) energy storage systems [11]. In bi-directional WPT, controlling the amount and direction of power flow is typically achieved through either phase or magnitude differences between the transmitter and receiver coils [12]. These differences are created by dedicated power converters on both sides, requiring effective control algorithms. While existing methods offer benefits like communication-free operation, they can also be complex. Additionally, considerations for magnetic design in bi-directional WPT systems have been explored in recent research [13], [14].

Among different designs for BWPT systems, a current-sourced approach is seen as ideal for facilitating V2G applications [15]. This system allows for power exchange between the grid and multiple independent devices. To control the grid current and maintain a stable DC voltage, a grid integrated bidirectional converter is used [16]. In contrast to unidirectional WPT systems, the suggested BWPT system demands more intricate control mechanisms. This complexity arises from the identical converter topologies and compensation networks on both ends, particularly when considering a single receiving unit. Typically, controlling the direction and amount of power flow relies on manipulating the voltage phase angle or magnitude produced by the converters. For battery charging applications, maintaining a specific active power level while minimizing reactive power is crucial [17]. However, detuned systems can suffer from variations in parameters and component tolerances, making this consistency difficult to achieve. To overcome this hurdle, a control technique relying on power-frequency droop characteristics has been suggested [18]. However, adopting this approach entails a trade-off, leading to heightened reactive power and volt-ampere rating as the operating frequency undergoes changes. The Series-Series (SS) compensation, known for its straight forward design and stable resonance frequency, is extensively utilized in high-power IPT systems, offering control over load and coupling factors [19]. Recognizing the impact of voltage and current on transmitter and receiver coils, achieving highly efficient WPT involves exploring various control algorithms. Conventionally, the regulation of output voltage or current in WPT systems involves employing phase shift control (PS), variable frequency control (VF), pulse density modulation (PDM) control, or alternative DC-DC converters [19], [20], [21]. However, challenges arise with VF and PS control, as achieving Zero Voltage Switching (ZVS) conditions across a wide load range proves difficult. However, efficiency is a major concern in BWPT systems, especially at high operating frequencies. Soft-switching the system across a wide range of voltages and loads is crucial for both efficiency gains and reducing electromagnetic interference. For unidirectional topologies, various methods have been proposed to ZVS on the primary inverter side [22]. These approaches include parameter tuning, control strategies, cascaded dc-dc converters, and incorporating controllable branches [23], [24], [25]. A key advantage of BWPT is the use of dual active bridges instead of a secondary rectifier. This allows for easy control of bidirectional power flow through phase-shifting and secondary bridge modulation for impedance tuning. Despite the introduction of a dual phase-shift (DPS) modulation strategy aimed at minimizing coupling coil losses, the challenge persists in achieving full soft-switching across a broad operating range [26]. Another strategy, the triple phase-shift (TPS) modulation, has been presented to tackle issues related to load matching and ensure zero voltage switching (ZVS) for all power switches throughout the entire power range [27]. However, this method neglects reactive current in its optimization, limiting further efficiency improvements. In Phase-Shift Modulation (PSM), a prevalent strategy for high-frequency inverters, adjusting the phase difference between leading and trailing bridge arms alters output voltage. Yet, this approach struggles with low loads and significant current harmonic components. Addressing the surging demand for EVs and the necessity for bidirectional power flow, PDM techniques have gained attention. Unlike traditional PWM, PDM adjusts energy transfer time during specific intervals, offering higher-resolution control, along with ZVS and Zero Current Switching (ZCS) tuning methods to enhance energy transfer efficiency. To achieve ZVS and ZCS for primary and secondary side converter switches, a conventional PDM technique regulates the output voltage. A proposed dual-side controlled system by H-Bridge inverter aims to boost overall efficiency without an additional DC-DC converter. Nevertheless, the effectiveness of this approach is impacted by the dependence of the SS compensation topology on coupling coil parameters. This reliance can potentially result in significant output voltage and current ripples due to prolonged PDM duration. The proposed PDM technique, applied for inverter

switching on both sides of the WPT system, enhances system efficiency, particularly under moderate load conditions. This method ensures constant switching frequency output voltage regulation and delicate shifting operation for high-frequency converter switches, requiring no additional components. The primary contributions outlined in the paper include:

- The FLC tuned dual side PDM technique for the BWPT system to provide better control and improved system performance.
- The performance of the proposed system is validated for the G2V and V2G modes of operation under different pulse density conditions and load variations.
- The circuit simulation and experimental prototype validation of the proposed FLC-PDM are performed for the BWPT system.

Section III describes the modes of operation of Pulse Density Modulation (PDM). Section IV elaborates on the Power Control using PDM techniques. Section V discusses the switching strategy sequence for pulse pattern identification in FLC-PDM. Section VI presents the simulation results during G2V and V2G mode of operation. Finally, the section VII discusses the experimental results and discussion.

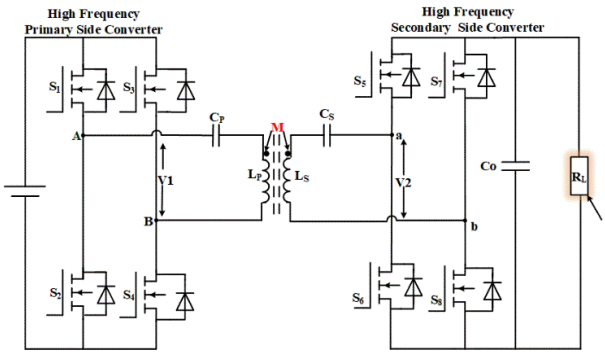

FIGURE 1. Block diagram of SS compensated BWPT system.

II. BIDIRECTIONAL POWER TRANSFER SYSTEMS

The SS compensation of the BWPT system is illustrated in Figure 1. A single-phase, voltage-fed inverter composed of four MOSFETs (S_1-S_4) is connected to a DC source. An equivalent series resonance (ESR) tank, consisting of C_P and L_P, is connected to the output of the inverter through a series resonant circuit, facilitated by a wireless charging coil with the coupling coefficient (K). The coefficient M represents the mutual inductance between the primary and secondary coils of the magnetic coupler.

The primary function of SS compensation is to operate resonantly at the switching frequency ω_S and can be described as follows:

$$L_pC_p = L_sC_s = \frac{1}{\omega_s^2} = \frac{1}{(2\pi f_s)^2} \tag{1}$$

Similarly, the coupling coefficient of the coil can be described as,

$$K = M\sqrt{L_PL_S} \tag{2}$$

where L_P and L_S are the inductance of the primary and secondary sides. The energy is transferred from the primary to the secondary terminals. The resonant circuit at the secondary side mirrors the primary side resonant circuit, and an H-bridge converter connection is established using four MOSFETs (S_5-S_8). The DC-link capacitor is denoted by CS, and the load resistance is denoted by R_L. The switching pairs of the primary and secondary sides are S_1&S_4, S_2&S_3 and S_5&S_8, S_6&S_7 respectively. The angular frequency is represented by the expression $\omega = 2\pi$fL, where ω is the angular frequency, f is the operating frequency and L is the inductance of coil. The converter and inverter switches are identical, that makes the current to flow in both forward and reverse directions between the primary and secondary sides. The fundamental harmonic approximation approach can be used to determine the fundamental components of current phasors, ignoring loss resistance, where,

$$I_1 = -j\alpha V_L; L_p - Lf_1 = \frac{1}{\omega_{S_1}^2 C_1} \tag{3}$$

$$i_2 = -j\alpha V_p; L_p - Lf_2 = \frac{1}{\omega_{S_2}^2 C_2} \tag{4}$$

From (3) and (4), it is described that the current phasors of a BIPT circuit with specified parameters are solely dependent on the output voltage of the other side's converter in a steady state. Figure 2 shows the equivalent circuit of the bidirectional WPT system. It consists of three impedances namely input impedance ZP, mutual impedance ZLM and output impedance ZS. From these values, equations of the primary and secondary parameters can be expressed as

$$Z_P = Z_{LM} + j\omega((L_P - L_M) - (\frac{1}{\omega_{C_P}^2})) \tag{5}$$

$$Z_S = R_{eq} + j\omega((L_S - L_M) - (\frac{1}{\omega_{C_S}^2})) \tag{6}$$

$$Z_{LM} = j\omega L_M \parallel L_S \tag{7}$$

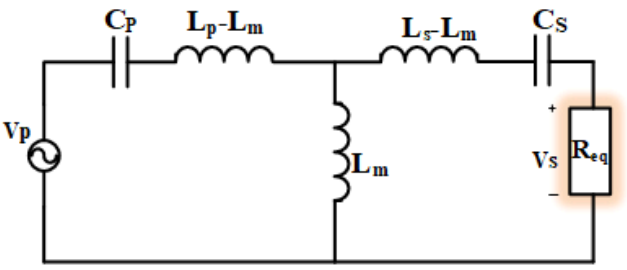

FIGURE 2. Equivalent circuit of the BWPT system.

III. PDM TECHNIQUE FOR POWER CONTROL

PDM offers two operational states: Injection Mode (IM) and Operational Mode (OM) [28]. In IM, two MOSFETs are turned on while the remaining two are turned off during each half-resonant cycle. Transitions from IM to OM involve energizing a single MOSFET while the others remain inactive.

Within each switching cycle, T_{ON} represents the duration of the active mode, while T_{OFF} represents the duration of the passive mode. The sum of these durations ($T_{ON} + T_{OFF}$) equals the total time period (T). The High-Frequency Converter functions as a standard diode bridge, delivering power to the load in the active mode. It switches control in the passive mode, where the output filter capacitor supplies the load, leading to a reduction in the output voltage.

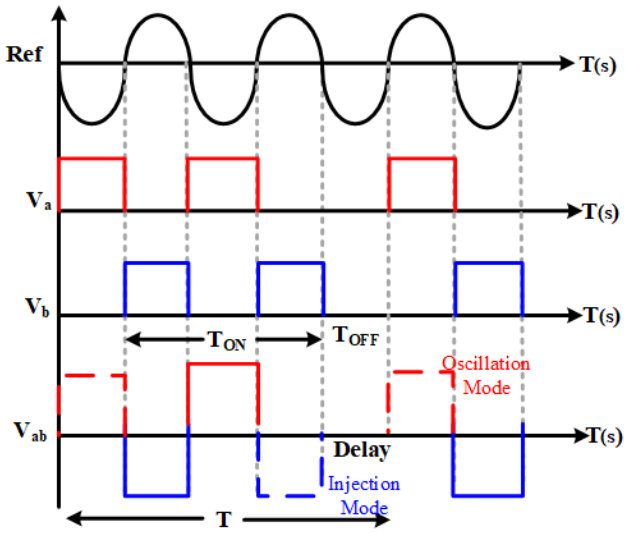

FIGURE 3. PDM-based power control operation.

The PDM technique maximizes the input voltage and current drawn from the high-frequency converter, as demonstrated by equations (8) and (9).

$$V_S = \frac{2\sqrt{2}V_o}{\pi} \times d \tag{8}$$

$$I_S = \frac{2\sqrt{2}V_o}{R_o} \times d \tag{9}$$

where (d) represents the Pulse Density can be expressed by the equation (10),

$$d = \frac{T_{ON}}{T_{PDM}} \tag{10}$$

Equation (11) conveys the following specification for the WPT system regular output power of the implementing the PDM technique

$$P_0 - P_{DM} = \frac{8V_0^2}{\pi^2 R_0^2} d^2 R_s = P_{\max}\left(\frac{T_{ON}}{T_{PDM}}\right)^2 \tag{11}$$

Equation (11) shows that adjusting the duty cycle (d) regulates the output power. The load receives its maximum power when d = 1. During the Operational Mode (OM) state of the PDM controller, the switches are remain in their transition conditions until the state changes. Figure 3 illustrates the control logic for the switches under PDM operation and the rectifier's input voltage waveform. The blue solid line in the figure represents the gate control signals for the active mode of switch conduction switches S_1 and S_4. Whereas the red dashed line representing the passive modes of the switches S_2 and S_4. Both converter voltages (V_P) and inverter voltages (V_S) can be represented as bipolar square waves. These waveforms consist of three distinct voltage levels: zero, positive, and negative. Various switching combinations of these levels are employed. The predetermined length of the PDM logic sequence defines the bipolar wave as a sequence of K total pulses. This sequence includes negative and positive square waves. Furthermore, an absence of oscillations is incorporated. Due to the time dependence of the PDM pulse sequence, it is possible to represent the voltage waveform V_{AB} with respect to time. The PDM Converter adjusts its RMS output voltage by repeating "run and stop" in accordance with a control sequence. The circuit waveform f(x), with a magnitude of V, can be expressed in trigonometric series form using the Fourier series described in equations (4) and (5). This expression is given as follows:

$$a_n = \frac{2}{T}\int_0^T Vf(x)\cos\frac{2\pi nx}{T}dx$$
$$\text{where n} = 0, 1, 2, 3, \ldots\ldots\infty \tag{12}$$

$$b_n = \frac{2}{T}\int_0^T Vf(x)sin\frac{2\pi nx}{T}dx$$
$$\text{where n} = 0, 1, 2, 3, \ldots\ldots\infty \tag{13}$$

Here, n indicates the n^{th} order of the Fourier-Series

$$\omega_0 = \frac{1}{2\pi\sqrt{LC}} \tag{14}$$

$$T = \frac{KT_0}{2} \tag{15}$$

The equation (14) & (15) representing the resonant frequency as ($\omega 0$) and (T) represent the period of the periodic pulse beginning with the K^{th} pulse.

IV. PDM MODE OF OPERATION

Here, the control technique keeps the frequency constant and adjusts the powering period to change the pulse density of the inverter. ZVS is achieved throughout the entire power control range due to the fact that the switching frequency cannot be changed. Concurrently, the MOSFETs S_2 and S_3 become active at the zero level with respect to the conduction of the switches S_1, S_4 on the primary side. Meanwhile, MOSFETs S_6 and S_7 become active at the zero level, whereas secondary side conduction enables the switching of MOSFETs S_5, S_8. The traditional PDM control method consists of solely two categories: active and passive modes. Modes I and II are referred to as the active mode or Injection mode, whereas Modes III and IV are known as the passive mode or oscillating mode. In Active Modes, the High-Frequency Converter functions at specific resonant cycles as a square-wave voltage source with an amplitude of V, whereas in the passive mode, it functions for some cycles as a zero-voltage source. To enable ZVS implementation, it is imperative to maintain a negative and positive current during the transition from

(-Vdc to +Vdc) and (+Vdc to -Vdc) of the output voltage. The input voltage (V_{REF}) is governed by the functioning of the MOSFETs on both the primary (S_1-S_4) and secondary (S_5-S_8) sides. The underlying principle of conventional PDM is to vary the pulse density of the control signals originating from the High-Frequency Converter at both terminals.

A. INJECTION MODE OR ACTIVE MODE(IM)

The switching pairs S_1 and S_4 are assigned on the primary side in the direction of current flow, while the switch pairs S_5 and S_8 are situated on the secondary side. On the primary side, current moves in a positive direction through S_1, capacitor C_1, the transmitter coil, and S_4. In contrast, on the secondary side, the current passes through the receiver coil, capacitor C_2, S_5, resistive load, and S_8. The duty cycle of switches has been selected as 50% on both the converter and inverter sides.

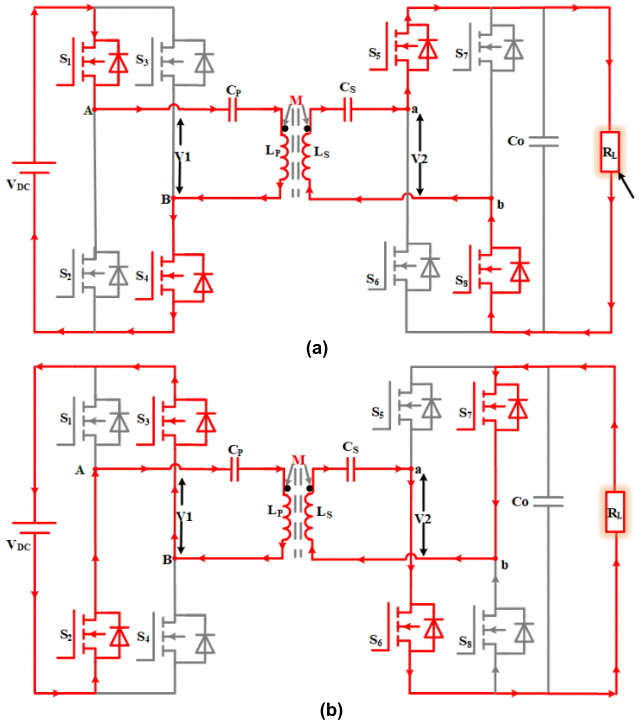

FIGURE 4. (a) Converter operates in positive (IM) mode (b) Converter operates in Negative (IM) mode.

As illustrated in Figure 4 (a), the switching position was modified in accordance with changes in the direction of the current. As power transfer is takes place from the input(primary) side to the output(secondary) terminal via a loosely coupled inductance, there is a surge in current, leading to an elevation in load voltage due to the charging of the DC capacitor. During the negative mode of IM, the current travels through the primary side via S_2, C_1, the transmitter coil, and S_3. Similarly, the current flows through the parallel capacitance (C_2), the switches (S_7, S_6), the resistive load, and the receiver coil on the secondary side, as shown in Figure 4 (b).

B. OSCILLATING MODE OR PASSIVE MODE (OM)

In OM mode, the gate turn-on signal is provided to a MOSFET positioned at the top or bottom limb, respectively, as depicted in Figures 5 (a) and (b). To provide a conducting path for the current, switches S_2 & S_4 at primary side and S_6 & S_8 in secondary side are activated in this mode. As power is transferred from the primary input side to the secondary output terminal through a loosely coupled inductance, an increase in current occurs. This surge in current results in a rise in load voltage, attributed to the charging of the DC capacitor. During the transition from IM to OM, the state of a single MOSFET is altered. The ZVS state can be achieved to the on-state MOSFET, similar to the Transition state. During the transition, an individual MOSFET modifies its conducting state, achieving ZCS.

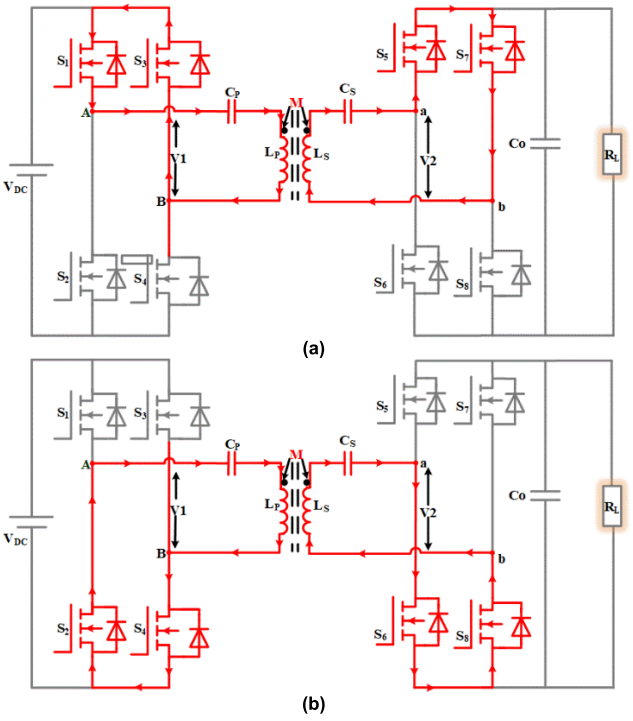

FIGURE 5. (a) Converter operates in OM (Upper Switch conduction) state (b) Converter operates in OM (Lower Switch conduction) state.

The primary (S_1&S_3) and secondary (S_5&S_7) switches are in the upper switching conduction state, with positive current flowing through the primary coil via switch S_1, parallel capacitor (C_1), the transmitter coil, via switch S_3, and the secondary coil through switches S_5 and S_7 via the parallel capacitor (C_2). As part of a control sequence, the PDM Converter cycles run and stop in order to modify the rms output voltage. During the transfer of power from the primary input side to the secondary output terminal through a loosely coupled inductance, an increase in current occurs, resulting in a rise in load voltage attributed to the charging of the DC capacitor. A negative current flow from the primary coil side through the, switch S_2, parallel capacitor (C_1), transmitter

coil, and switch S_4, and vice versa for the secondary coil through switches S_6 and S8 via the parallel capacitor (C_2).

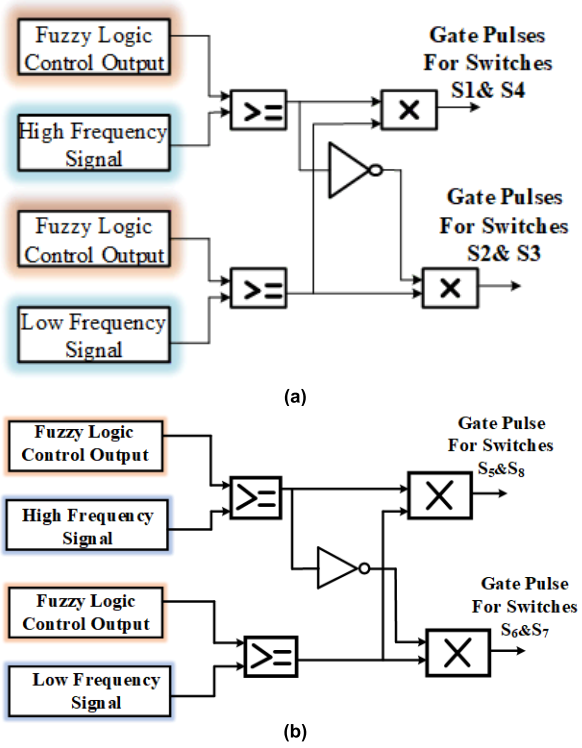

FIGURE 6. (a) Block diagram of gate Pulse generation for primary side converter (b) Block diagram of gate Pulse generation for Secondary Side Converters.

V. FUZZY LOGIC CONTROL-BASED SWITCHING STRATEGY FOR PDM

For improving the effectiveness and performance of wireless power transfer systems is achieved by using the Fuzzy Logic Control-Based Switching Strategy for PDM in BWPT system. This approach uses fuzzy logic control to optimize the PDM technique's switching decisions, making it especially suitable for bidirectional power transfer applications. Fuzzy logic allows the control algorithm to be more adaptive to changing and unpredictable operating conditions by allowing human-like reasoning and decision-making to be incorporated. The PDM technique involves maintaining a constant inverter switching frequency slightly higher than the load resonant frequency to minimize switching losses. Figure 6 shows a logic circuit that generates pulses for inverter switches. The gate signals for MOSFETs S1 through S4 on the primary side and MOSFETs S5 through S8 on the secondary side converters are illustrated in Figures 6(a) and (b), respectively. The process involves logically contrasting pulse signals with high frequencies (85 kHz) and low frequencies (80 Hz). The PDM controller's duty cycle is defined as:

$$\alpha_{PDM} = \frac{t_{ON}}{t_{PDM}} \tag{16}$$

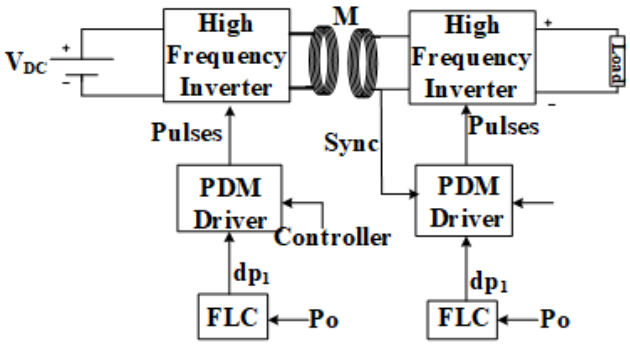

FIGURE 7. Block diagram of Series-Series (S-S) Compensated FLC- PDM Controlled BWPT system.

where (ton) and (toff) represent the time periods during which the PDM pulses transition from On to Off, respectively.

The duty cycle (D) is determined by the output power (P_O) or from the output voltage and current value. The D value changes based on the difference between the reference value (P_{ref}) and the actual value. Figure 7 illustrates the block diagram to control the BWPT system for the proposed converter using FLC-PDM. The proposed technique regulates the output voltage of an inverter/rectifier, eliminating the need for a dc-dc converter.

This process modulates the pulse density of the inverter's switching signals, ensuring constant switching loss across the load range due to the absence of variation in the switching frequency. Figure 8 illustrate the flowchart to generate the duty cycle based on fuzzy system. The focus was directed towards the four resonant cycles, resulting in the converter's output voltage being a periodic waveform. In this waveform, the average output voltage corresponds to 3/4 when compared to full power operation, as indicated by equations (17) and (18).

$$D = \frac{T_{ON}}{T} = \frac{3}{4} \tag{17}$$

$$T = NT_r = T_{ON} + T_{OFF} \tag{18}$$

The resonant circuit (V_{AB}) enters a zero-voltage state when the fourth cycle shows an off-period (T_{OFF}) in the resonant converter. It operates in modes I and II, producing square wave voltages oscillating between (+Vab and -Vab) during the period of [T_{ON}], which comprises three resonant cycles. This is referred to as Oscillation Mode (OM) or Passive Mode. Table 1 provides the fuzzy table for duty cycle generation for PDM pulses, offering the range of duty cycle to be generated for the optimal PDM pulse width. Fuzzy logic presents an approach to adaptively control indeterminate and non-linear issues. The FLC requires two input parameters: error (PO) and the change in error (ΔPO), and a single output parameter (DPDM). The triangular membership function (MF) is chosen to describe variables (PO, ΔPO, DPDM) in the range [−1, 1], as illustrated in Figure 9. Table 1 displays the rule base, encompassing seven membership functions identified as LN, MN, SN, Z, SP, MP, and LP. Each of these

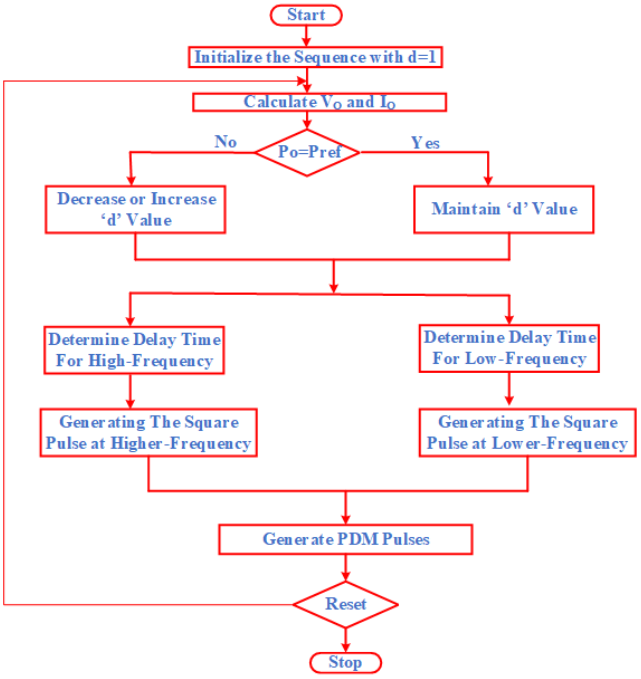

FIGURE 8. Fuzzy-PDM control strategy.

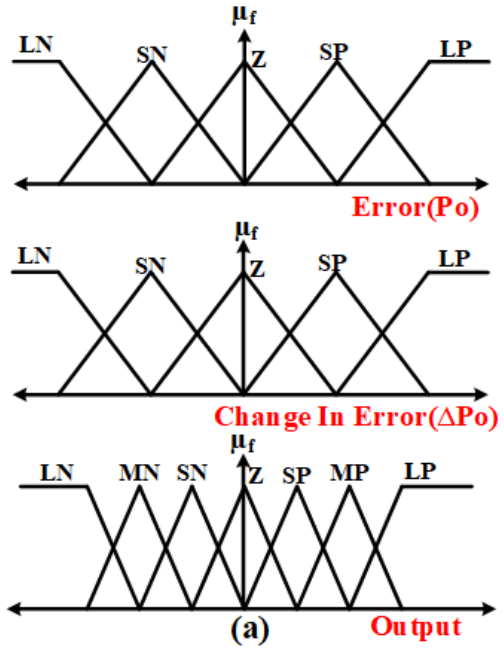

FIGURE 9. FLC's membership function input and output parameters.

functions corresponds to the respective classifications: zero, small positive, medium positive, and large positive.

In accordance with the rule basis, the PDM pulses for the inverter switches are generated using the control signal supplied by FLC. The designed FLC will regulate the modulation index (D_{PDM}) in order to monitor the specified power. The FLC with 7 MF has lower time domain specifications with optimum rules, while the controller with 9 MF has similar results but requires an increased number of rules, requiring more space and time for computation. Therefore, 7 MF continues to be the most effective and preferred selection in this article as illustrated in Table 1.

TABLE 1. Fuzzy system for duty cycle generation for PDM.

Po/ΔPo	LN	MN	SN	Z	SP	MP	LP
LN	LN	MN	SN	SP	MP	LP	Z
MN	MN	SN	SP	MP	LP	Z	LN
SN	SN	SP	MP	LP	Z	LN	MN
Z	SP	MP	LP	Z	LN	MN	SN
SP	MP	LP	Z	LN	MN	SN	SP
MP	LP	Z	LN	MN	SN	SP	MP
LP	Z	LN	MN	SN	SP	MP	LP

Consequently, by changing the pulse density of the square wave voltage, it is possible to regulate the output power of the converter. By continuously operating all MOSFETs at zero current, lower frequency control in the PDM can significantly reduce switching losses. The converter's output voltage displays a periodic waveform over four resonant cycles, allowing precise control of output power by adjusting pulse density. The continuously cycling nature of each MOSFET at zero current significantly reduces switching losses compared to control based on lower frequency pulses. The investigation involves a switching pattern consisting of active and passive modes for each pulse.

In a typical SS topology application, voltage fluctuations may occur due to load resistance changes. To uphold voltage stability, it is essential to fine-tune the pulse density D, and the overall efficiency hinges on the collective impact of pulse sequences. The finite solution for the arrangement of IM and OM states can be achieved across various densities by integrating the respective configurations. The design phase procedure involves computing efficiency for each combination to identify the optimal pulse sequence for each density.

Stage 1: Determine the K value of the PDM sequences

Stage 2: To generate the pulse combinations with a specified density within a K-length sequence, expressing voltages (VINV), and (VRECT) in different forms using the combination definition.

Stage 3: Optimal power transfer efficiency at a standard pulse-density D can be chosen by utilizing the outcomes from the earlier stage 2 and incorporating them into efficiency calculation processes with the utilization of measured system parameters.

Stage 4: Attaining the most efficient Pulse Density Modulation (PDM) sequence involves integrating different pulse densities D together into the aforementioned steps. The sequence of the PDM is identified as containing a specific quantity of K pulses, and the proportion of IM states within the generated sequence is denoted by the pulse density D.

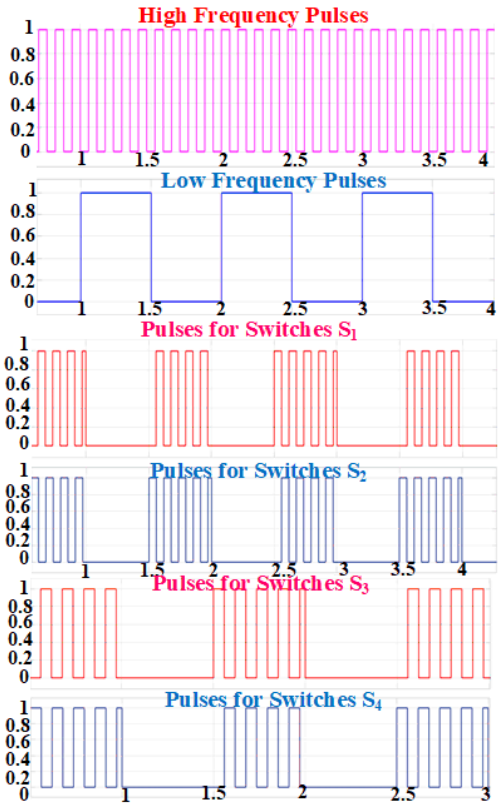

FIGURE 10. (a) The PDM control Gate Pulse Sequence of High Frequency Primary Side Converters Mosfet Switches (S1-S4). (b) The PDM control Gate Pulse Sequence of High Frequency Secondary Side Converters Mosfet Switches (S5-S8).

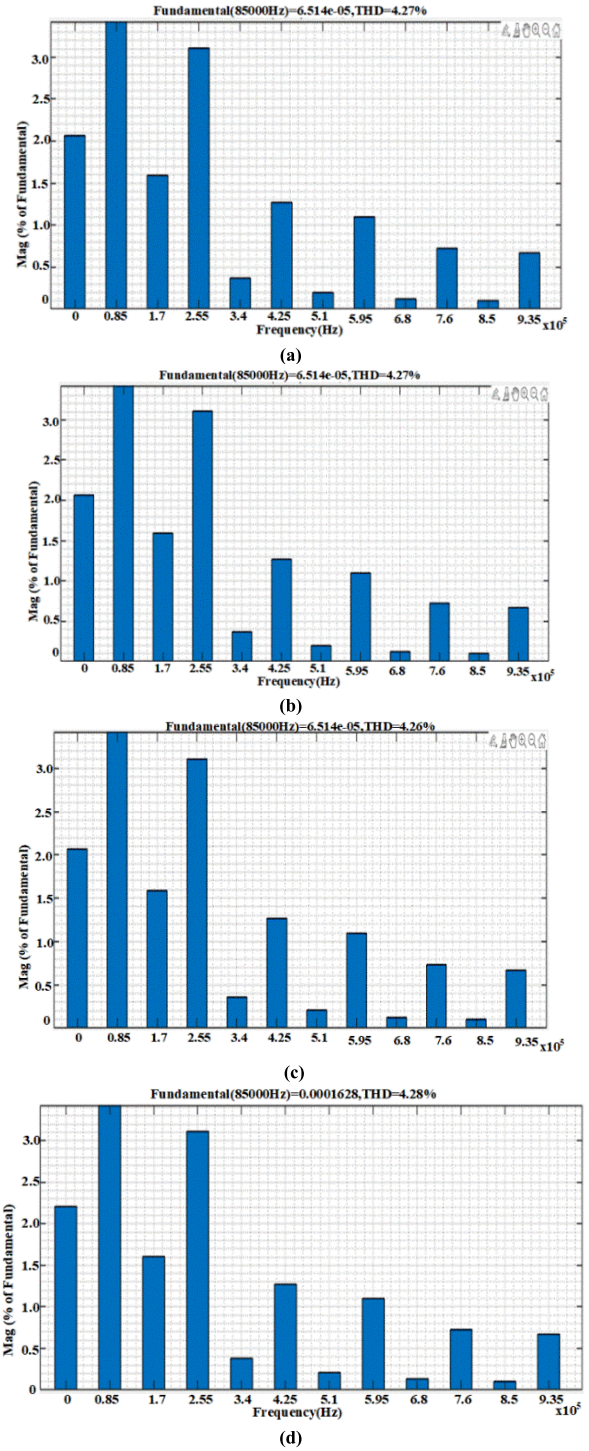

FIGURE 11. (a) THD of Transmitter Coil Side Current for G2V operation (b) THD of Receiver Coil side current (c) THD of Transmitter Converter Side Current for G2V operation (d) THD of Receiver Converter side current for G2V operation.

Equation (19) provides an equation for calculating the combined quantity current(I) for each density

$$I = C_K^{(1-D)K}, D \in [0, 1] \tag{19}$$

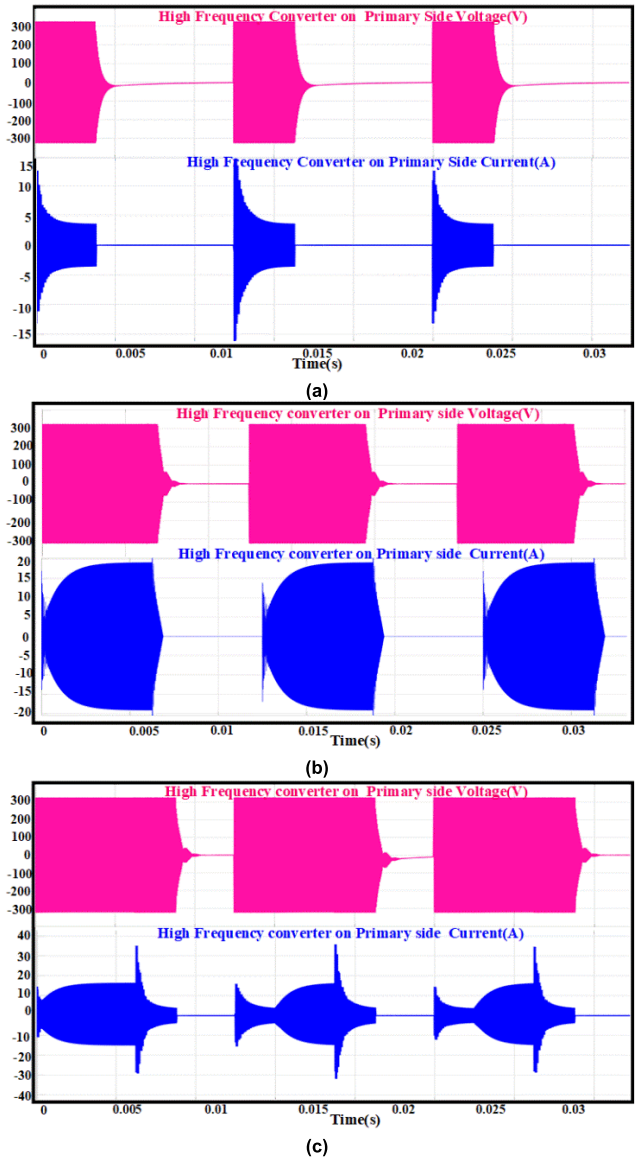

FIGURE 12. Voltage and Current waveforms of Primary side of Converter in Charging Mode (G2V) of operation (a) $\delta = 30\%$ (b) $\delta = 50\%$ (c) $\delta = 70\%$.

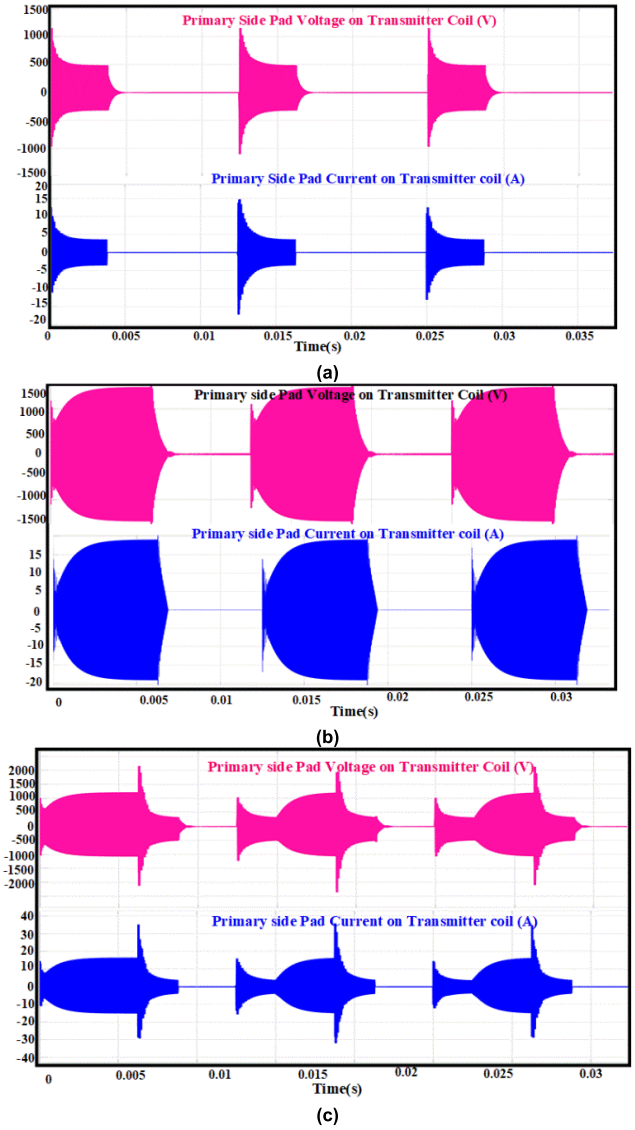

FIGURE 13. Voltage and Current waveforms of Primary side of Transmitter Coil Pad in Charging Mode (G2V) of operation (a) $\delta = 30\%$ (b) $\delta = 50\%$ (c) $\delta = 70\%$.

Consequently, the formula (20) can be employed to articulate the total count of combinations that necessitate computation.

$$A = \sum_{D \in [0,1]} I \tag{20}$$

The modulator adjustment step P and the quantity K are interconnected through the equation (21)

$$\mathrm{P} = 1/\mathrm{K} \tag{21}$$

As per equation (21), it is evident that a greater number of pulses in the sequence leads to an increased computational workload. Simultaneously, it is observed that the adjustment step P is inversely proportional to K. Therefore, striking a balance between adjustment precision and computational load becomes crucial. Equation (21) elucidates that the computational workload rises with an increase in the number of pulses in the sequence. Conversely, the relationship between K and the adjustment step P can be mathematically expressed as inverse proportionality. Thus, achieving a balance between calculation quantity and adjustment precision is necessary.

VI. SIMULATION RESULTS

A Simulink model was developed in MATLAB to simulate a SS compensated BWPT system using Fuzzy-PDM control. The proposed system parameters were set to design for 3.7 kW power and resonance frequency of 85 kHz. The inverter supplied a 325 V DC input voltage, and the PDM frequency was chosen to be 85 Hz. Detailed circuit parameters can be found in Table 2. The switching frequency of the IPT converter was determined through simulation to match the resonance frequency (85 kHz) with a load resistance of

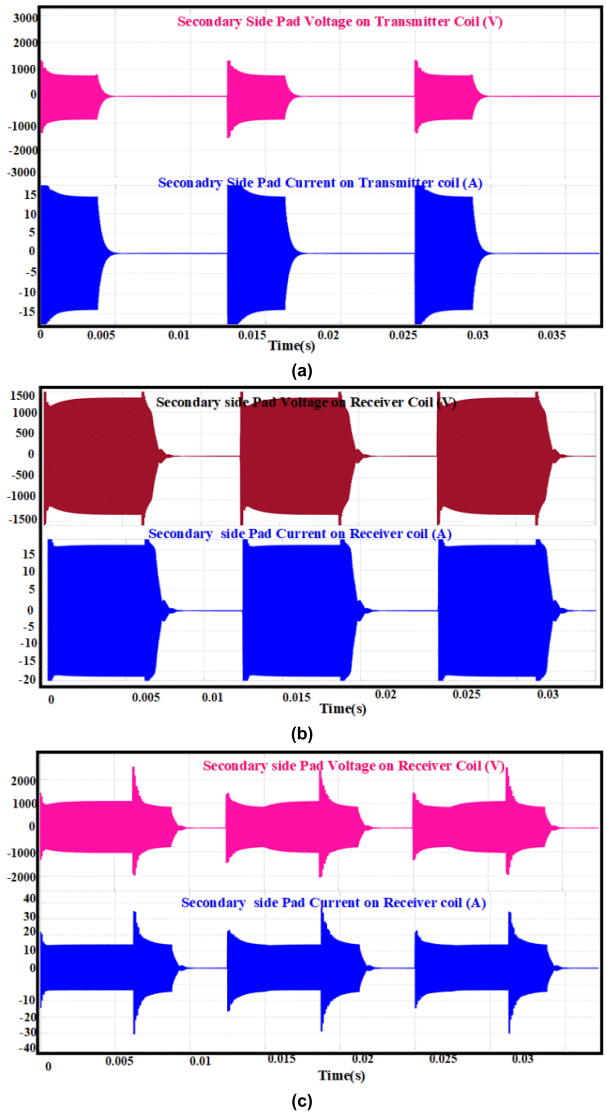

FIGURE 14. Voltage and Current waveforms of Secondary side of Receiver Coil Pad in Charging Mode (G2V) of operation (a) $\delta = 30\%$ (b) $\delta = 50\%$ (c) $\delta = 70\%$.

TABLE 2. Electrical circuit parameters for BWPT Systems.

S: No	Parameters	Symbols	Values
1	Input DC Voltage	V_{DC}	325 V
2	Load Voltage	V_{out}	360 V
3	Coupling Co-efficient	K	0.1- 0.4
4	Switching Frequency	f_s	85 kHz
5	Mutual Inductance	M	46.4 µH
6	Primary Side Series Compensation Capacitor	C_p	31 nF
7	Self-Inductance of the Primary Coil	L_p	116 µH
8	Self-Inductance of the Secondary Coil	L_s	116 µH
9	Secondary Side Series Compensation Capacitor	C_s	31 nF
10	Capacitance Filter	C_0	27 µF
11	Load Resistance	R	35 Ω

35 Ω. Both the converter-side switches (S_1-S_4) and (S_5-S_8) are operated at different duty ratios of the PDM signals.

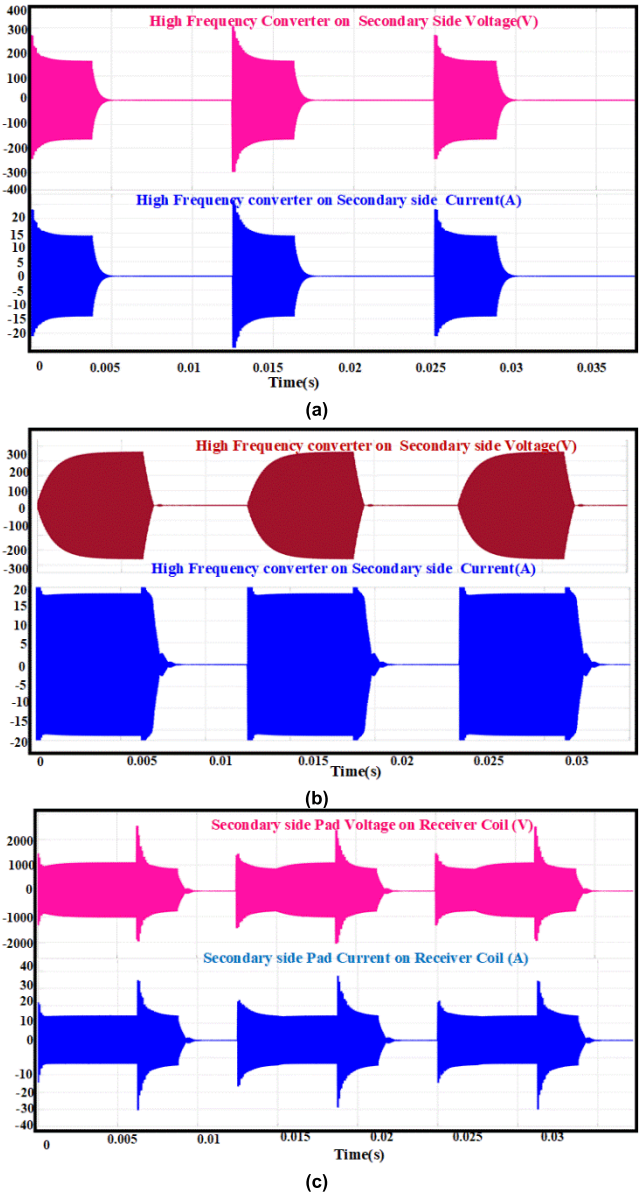

FIGURE 15. Voltage and Current waveforms of Secondary side of Converter in Charging Mode (G2V) of operation (a) $\delta = 30\%$ (b) $\delta = 50\%$ (c) $\delta = 70\%$.

The resulting Total Harmonic Distortion (THD) for the 85 kHz switching frequency was 4.27% on the transmitter coil side and 4.28% on the receiver coil (G2V side), as illustrated in Figures 11(a), (b), (c) and (d). The THD at the coil and converter side is below the 5% range only. Moreover, the fundamental and third harmonic components are only dominating in the system. The duty ratio and pulse density are varied based on the load voltage and current. The triangular membership function is used to tune the density with Fuzzy rule base.

A. POWER FLOW FOR G2V (CHARGING MODE)

The G2V simulation is performed for the duty of 30%, 50% and 70% and the voltage and current across the primary side

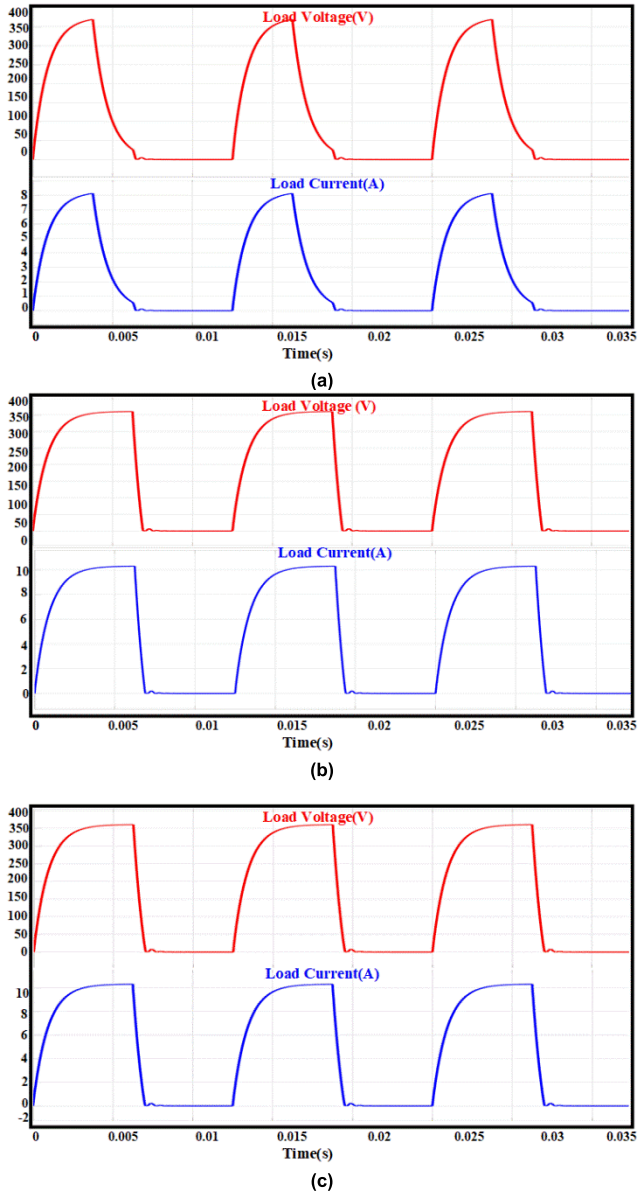

FIGURE 16. Voltage and Current waveforms of Load in Charging Mode (G2V) of operation (a) $\delta = 30\%$ (b) $\delta = 50\%$ (c) $\delta = 70\%$.

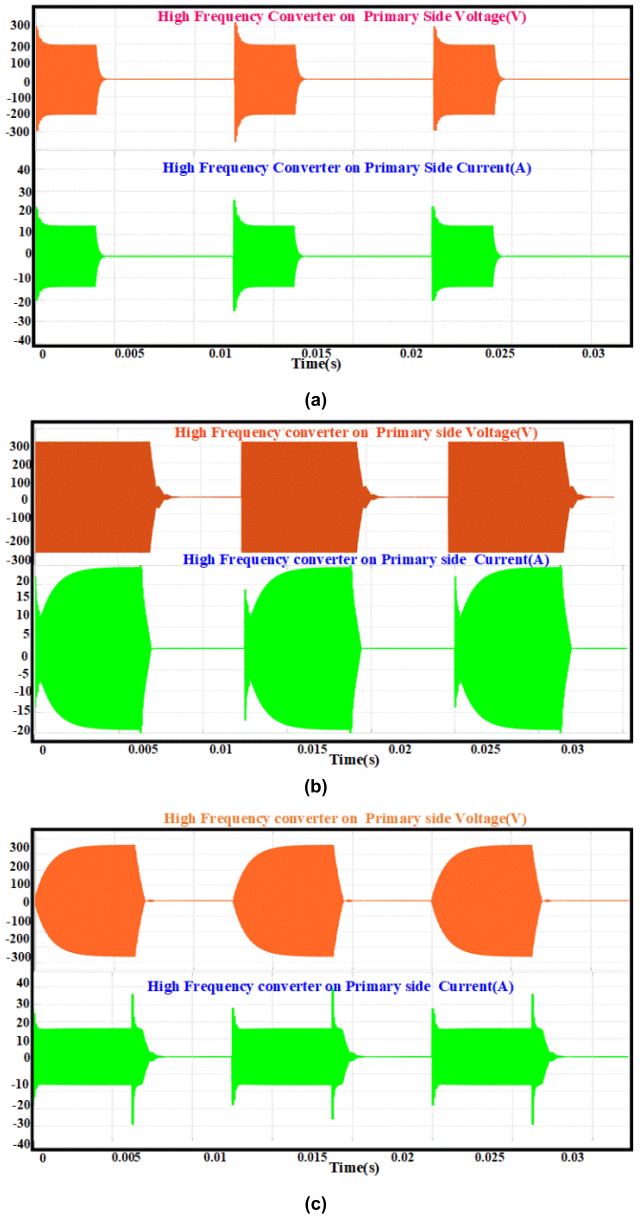

FIGURE 17. Voltage and Current waveforms of Primary side converter in Discharging Mode (G2V) of operation (a) $\delta = 30\%$ (b) $\delta = 50\%$ (c) $\delta = 70\%$.

converter and coil are measured. The simulation results show the effective power transfer changes as the density of the waveform changes. Figure 12 and 13 illustrates the primary side converter and coil voltage and current.

As the density of the waveform increases the duty ratio changes accordingly or vice versa. The measured voltage waveform across the converter is not having spikes, whereas the current waveform shows that the increase in the spikes for the higher duty ratio condition. It indicates the excess of stored energy circulation across the resonant tank. Similarly, the voltage and current waveform measured across the primary pad shows the voltage and current spikes at the starting and ending cycle of the waveform. The measurements are performed at the secondary side of the BWPT system as illustrated in the Figure 14 and Figure 15. The simulations are performed under different duty ratio of the pulse density conditions. Similarly, the current and voltage waveforms for the secondary converter and coil sides are captured under G2V mode of operation.

The measured voltage and current indicates that the switching (ON & OFF) time varies depending on the output power requirement. The ideal technical solution for ensuring ZVS in Fuzzy-PDM control is variable switching frequency control that approaches the resonance frequency during zero-crossing instants. To attain the ZVS condition, the switching PWM frequency of the high-frequency converter is kept constant at 85kHz. In contrast to frequency and duty cycle adjustments,

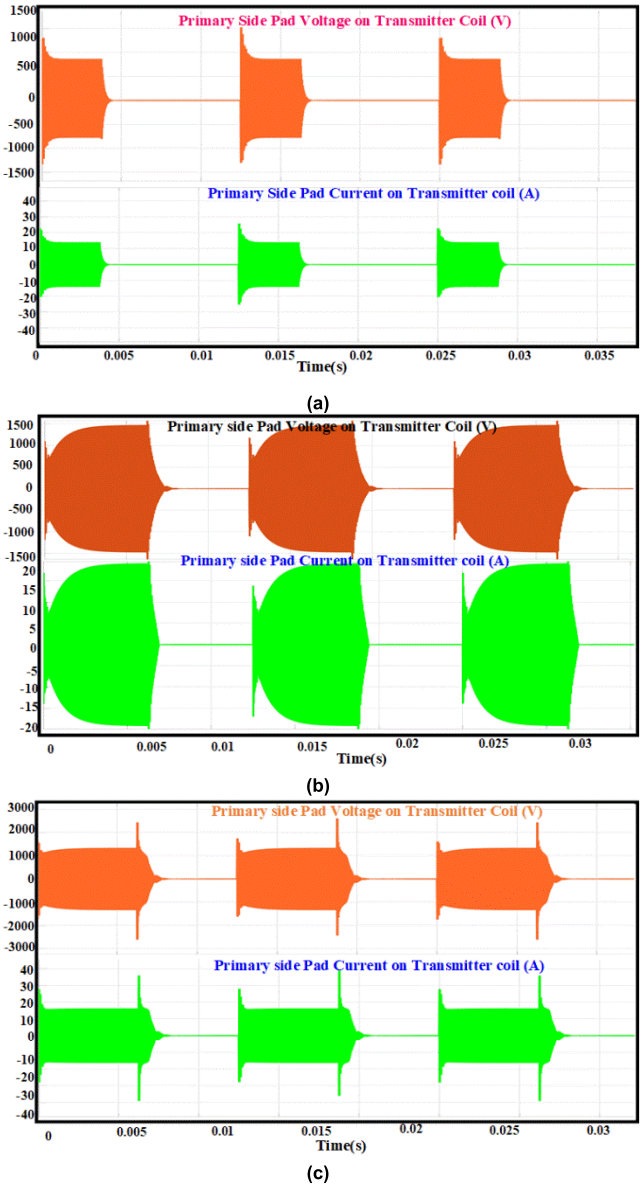

FIGURE 18. Voltage and Current waveforms of Primary side coil in Discharging Mode (G2V) of operation (a) $\delta = 30\%$ (b) $\delta = 50\%$ (c) $\delta = 70\%$.

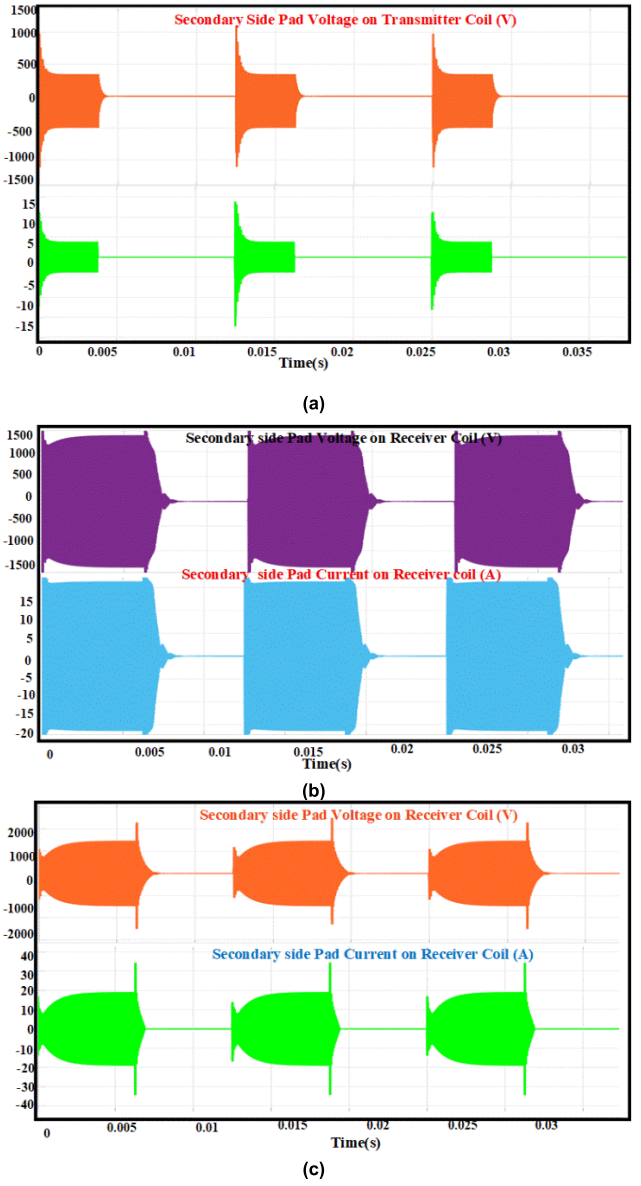

FIGURE 19. Voltage and Current waveforms of Secondary side coil in Discharging Mode (G2V) of operation (a) $\delta = 30\%$ (b) $\delta = 50\%$ (c) $\delta = 70\%$.

this method functions in a soft-switching mode through density manipulation of the high-frequency pulses. The voltage across the receiver pad is over 1200 V and current is of 15 A and the effective power changes based on the density of the pulse supplied to the primary converter.

The power transfer to the secondary side the converter is varied based on the coupling factor and the pulse density condition. For the 50% duty cycle the secondary side converter voltage and current are 360 V and 18 A. As the duty ratio is adjusted to the 30% and 70% of the cycle the overall power transferred to the load also varied as indicated in the Figure 15(a) and (c). The voltage and current spikes are present during the transition period of the PDM changes from 50 to 70% or 30%. The secondary converter is having lesser impact on the voltage spikes as compared to the current transition. As the converter output is connect to the filter capacitor across the load unit. The power supplied to the load is adjusted using the secondary PDM also, irrespective of the primary control.

The load voltage and current waveforms of the G2V charging mode systems are illustrated in Figures 16. The equivalent load is modelled with the resistance of 35 Ω based on the calculation. The waveform shows that the measured voltage and current for the different duty cycle are in the order of 360 V and 10 A. The effective power across the load changes as per the percentage of the duty ratio. For the fluctuations across the load voltage and current are eliminated with the use of filter capacitor at the output of the secondary side converter.

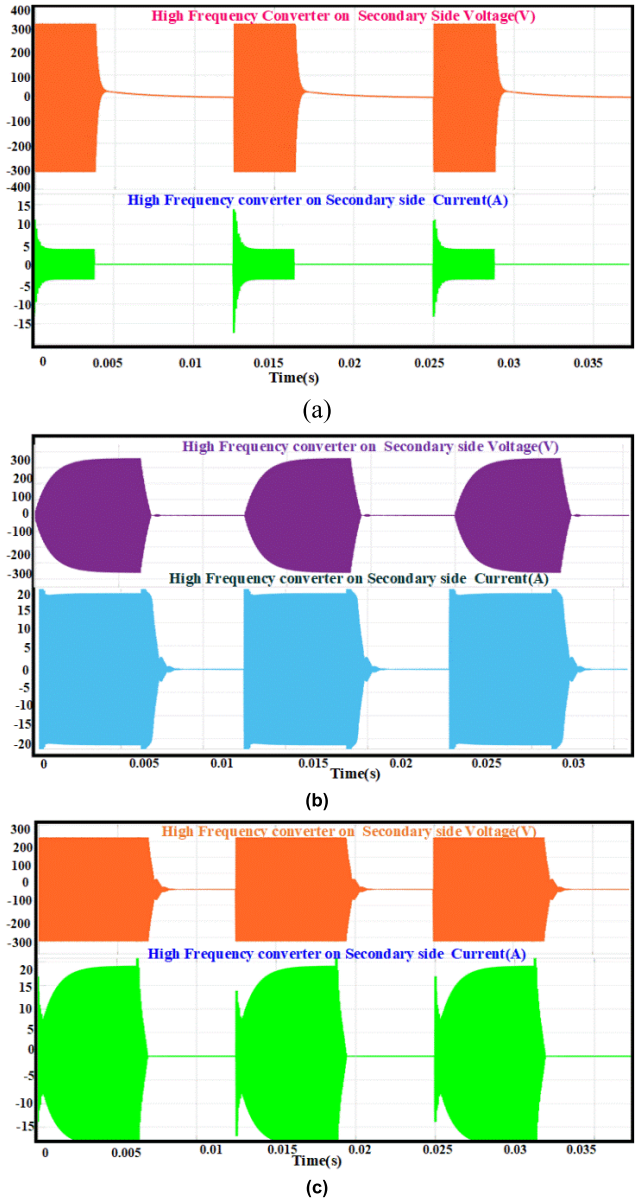

FIGURE 20. Voltage and Current waveforms of Secondary side converter in Discharging Mode (G2V) of operation (a) $\delta = 30\%$ (b) $\delta = 50\%$ (c) $\delta = 70\%$.

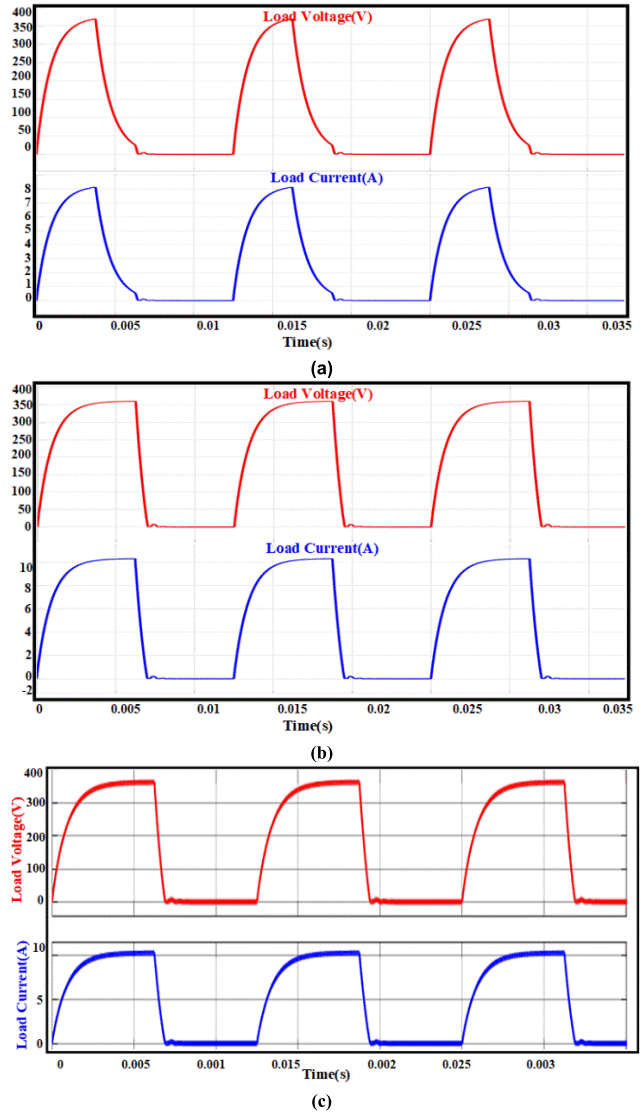

FIGURE 21. Voltage and Current waveforms of Load in Discharging Mode (G2V) of operation (a) $\delta = 30\%$ (b) d $\delta = 50\%$ (c) $\delta = 70\%$.

Moreover, the filter capacitor also provides better stabilization during the reverse operation of the BWPT system. The power transfer to the load depends on the duty ratio, coupling factor as well as the load resistance.

B. POWER FLOW FOR V2G (REVERSE SIDE)

This study investigates the impact of duty cycle on a Vehicle-to-Grid (V2G) simulation. The experiment measures voltage and current across the primary side converter and coil at three duty cycles: 30%, 50%, and 70%. The results show that changes in waveform density (pulse density) affect the efficiency of power transfer. Figures 17 and 18 illustrate the voltage and current waveforms across the primary side converter and coil. As the duty ratio increases or decreases, the converter adjusts accordingly. Notably, the converter's voltage waveform remains smooth, while the current waveform exhibits increasing spikes at higher duty cycles. This

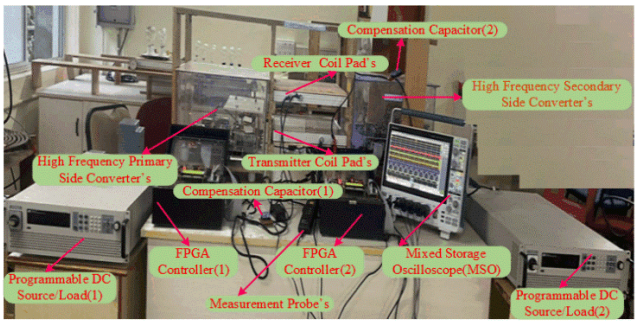

FIGURE 22. Experimental prototype setup of the proposed BWPT system.

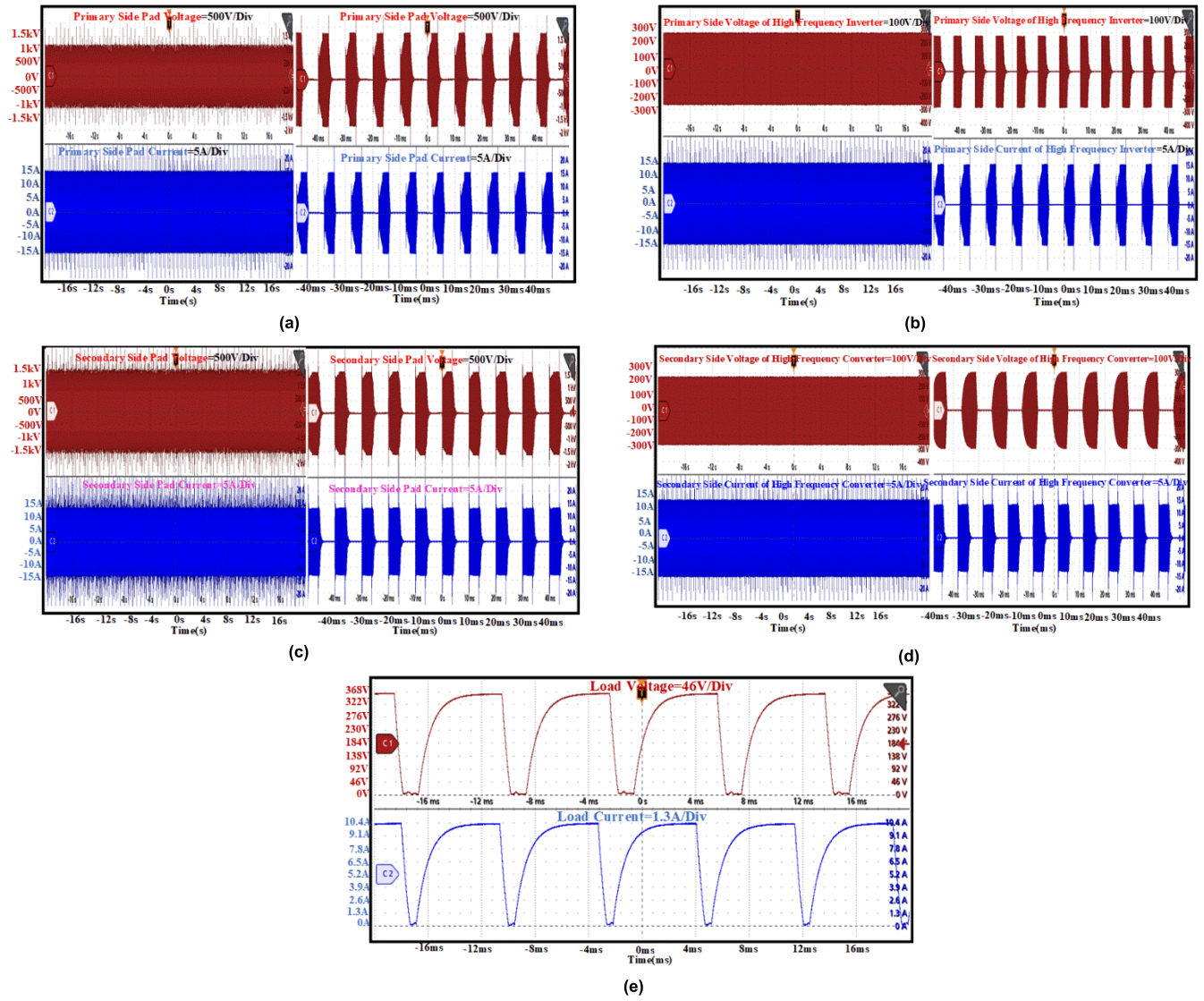

FIGURE 23. Charging mode of G2V system (a) Transmitter coil side Voltage and current (b) Primary converter side Voltage and current (c) Receiver coil side Voltage and current (d) secondary converter side Voltage and current (e) Load voltage and current.

suggests the circulation of excess stored energy within the resonant tank. Similar observations are made on the secondary side of the Bidirectional Wireless Power Transfer (BWPT) system, as shown in Figures 19 and 20. Here, current and voltage waveforms measured across the secondary converter and coil also exhibit spikes at the beginning and end of the waveform cycle. These simulations are conducted under various duty ratios for the pulse density modulation. Additionally, voltage and current waveforms are recorded for the secondary converter and coil during Vehicle to Grid (V2G) operation.

Figures 21 illustrate the load voltage and current waveforms for the V2G charging mode. The equivalent load is modeled as a 35 Ω resistor based on calculations. The waveforms show measured current and voltage values in the range of 360 V and 10 A, respectively, for different duty cycles. The effective power delivered to the load varies with the duty cycle percentage. A filter capacitor at the output of the secondary side converter eliminates fluctuations in the load voltage and current. This capacitor also enhances stability during the BWPT system's reverse operation (G2V). The power transferred to the load depends on three key factors: duty ratio, coupling coefficient, and load resistance.

VII. HARDWARE RESULTS

The prototype of the BWIPT system is designed as per the rating specified in Table 1 to validate the performance of the proposed Fuzzy-PDM approach. The proposed BWPT components with substantial power consumption are the primary side inverter, compensation inductor, and coupling coils, respectively. By implementing ZVS on both sides of the high-frequency converter, switching losses are minimized.

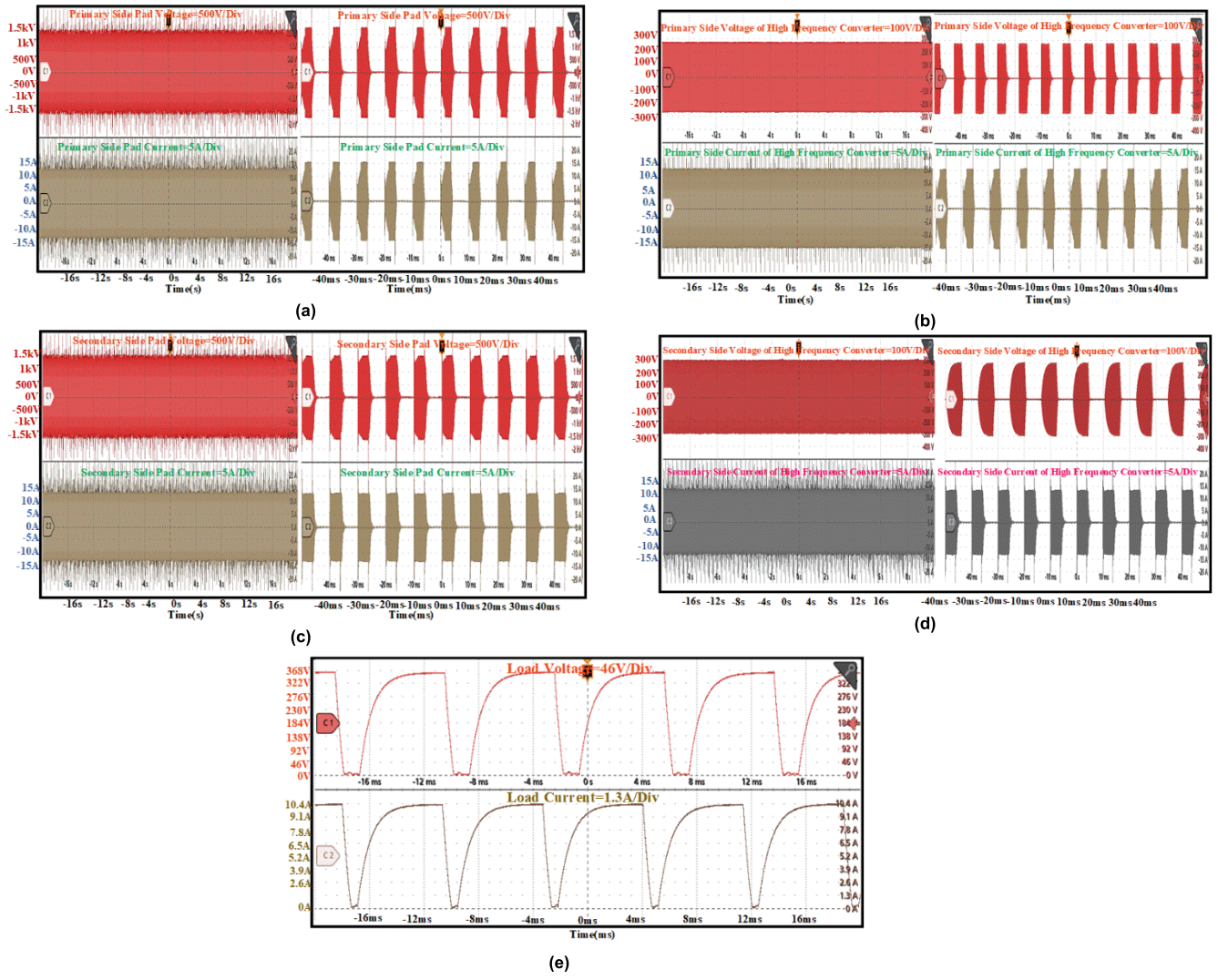

FIGURE 24. Discharging Mode of V2G system (a) Transmitter coil side Voltage and current (b) Primary converter side Voltage and current (c) Receiver coil side Voltage and current (d) secondary converter side Voltage and current (e) Load voltage and current.

A constant switching frequency of 85 kHz is maintained for the transmitter side converter. The performance of the Fuzzy-PDM approach were evaluated for different pulse density values. As the power losses are frequency-dependent, and the equivalent switching frequency is directly proportional to pulse density. The input and output voltage are 325V and 360V, respectively, and the load resistance is 35 Ω. For full load operation, the output current is 10A. Normally, a 150 mm air gap has to be created between the primary and secondary pads. The Litz-Wire (with a strand diameter of 0.1 mm) are employed to develop the coupling coils to minimize the skin and proximity effects. The coils on the primary and secondary sides of the inductors are squarely wound with Litz wires to decrease the ESR. The coupling coefficient between the charging pad is maintained constant by keeping the distance between the coil as per the ground clearance norms. The high-frequency inverter for both sides is managed by the Field Programmable Gate Array (FPGA SPARTAN 6) via a PWM signal operating at 85kHz and a 50% duty ratio. Due to resonance conditions, high voltage is generated across the resonant inductor.

Consequently, the resonant inductor is equipped with an air coil. Silicon carbide (SiC) MOSFETs C2M0040120D are preferred for high-frequency converters with a full-bridge inverter, capable of withstanding voltages of 1200V and currents of 60A. The TEKTRONIX (A622) current probe measures AC and DC current signals with 100 Amps and 70 Amps RMS, while the TEKTRONIX (MSO44 4-BW-500) displays voltage and current waveforms.

Figures 23 and Figure 24 illustrate the experimental current and voltage waveforms across the receiver and transmitter coils side, evaluated at 50% of duty ratio conditions for G2V & V2G operation. Whereas the suggested Fuzzy-PDM is implemented across the output and input terminals of the charging pads using high frequency converters. The pulse density is reduced to 50% to maintain a constant output

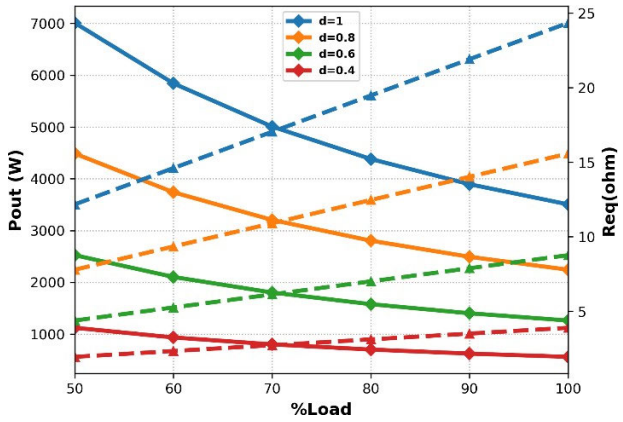

FIGURE 25. Equivalent resistance and output power for various duty cycles.

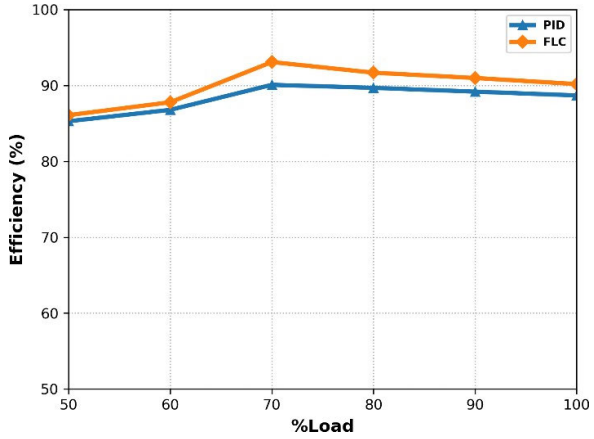

FIGURE 26. Comparison of efficiency for various loads with PI and FLC based PDM approach.

voltage. The Fuzzy-PDM inverter produces zero-voltage conditions, resulting in no transition in a MOSFET, leading to a significant decrease in the average switching frequency and reduced switching loss. The proposed Fuzzy-PDM shows increased efficiency with reduced output voltage ripple due to the short-duration operation during PDM control. The effectiveness of the Fuzzy-PDM method was assessed under a load condition of 50%, where it produced a maximal output power of 3.7kW while maintaining an efficiency of 93.1%.

The performance of the FLC-PDM based BWPT system where evaluated under different load regulations and the equivalent load resistance. The duty ratio is adjusted to vary the pulse density, the measured output load power is plotted in the Figure 25. Similarly, the efficiency of the developed FLC-PDM and PID controlled PDM were compared under different load conditions as illustrated in Figure 26. The peak efficiency of the proposed approach is achieved around 93% and maintains higher than PID for various load conditions.

VIII. CONCLUSION

In conclusion, this manuscript presents a novel solution specifically designed for BWPT systems using FLC-PDM technique. FLC-PDM, which is essential for G2V and V2G functions to maximize power transfer efficiency by addressing flaws in current modulation approaches. The technique uses a fuzzy rule base in conjunction with dual-side pulse density control to provide smooth load demand adaptability. Notably, FLC-PDM accomplishes output voltage regulation, delicate shifting operations, and consistent switching frequency for high-frequency converter switches without the need for extra parts. Extensive circuit calculations and hardware testing at 85 kHz frequency and 3.7 kW power demonstrate that the FLC-PDM technique achieves an efficiency of more than 93% for a variety of pulse densities and load resistances. Moreover, the FLC-PDM is a flexible and resilient solution that can improve bidirectional control in BWPT systems. This might lead to breakthroughs in smart grid technology and the integration of EV, which will be important for a sustainable energy future.

REFERENCES

[1] W. Lyu, Y. Hu, J. Liu, K. Chen, P. Liu, J. Deng, and S. Zhang, "Impact of battery electric vehicle usage on air quality in three Chinese first-tier cities," *Sci. Rep.*, vol. 14, no. 1, pp. 1–18, Jan. 2024, doi: 10.1038/s41598-023-50745-6.

[2] X. Zhang, Y. Wang, X. Yuan, Y. Shen, Z. Lu, and Z. Wang, "Adaptive dynamic surface control with disturbance observers for battery/supercapacitor-based hybrid energy sources in electric vehicles," *IEEE Trans. Transport, Electrific.*, vol. 9, no. 4, pp. 5165–5181, Oct. 2022, doi: 10.1109/TTE.2022.3194034.

[3] X. Zhang, Z. Wang, and Z. Lu, "Multi-objective load dispatch for microgrid with electric vehicles using modified gravitational search and particle swarm optimization algorithm," *Appl. Energy*, vol. 306, Jan. 2022, Art. no. 118018, doi: 10.1016/j.apenergy.2021.118018.

[4] X. Zhang, Z. Lu, X. Yuan, Y. Wang, and X. Shen, "L2-gain adaptive robust control for hybrid energy storage system in electric vehicles," *IEEE Trans. Power Electron.*, vol. 36, no. 6, pp. 7319–7332, Jun. 2021, doi: 10.1109/TPEL.2020.3041653.

[5] M. Hou, Y. Zhao, and X. Ge, "Optimal scheduling of the plug-in electric vehicles aggregator energy and regulation services based on grid to vehicle," *Int. Trans. Electr. Energy Syst.*, vol. 27, no. 6, p. e2364, Jun. 2017, doi: 10.1002/etep.2364.

[6] M. Shirkhani, J. Tavoosi, S. Danyali, A. K. Sarvenoee, A. Abdali, A. Mohammadzadeh, and C. Zhang, "A review on microgrid decentralized energy/voltage control structures and methods," *Energy Rep.*, vol. 10, pp. 368–380, Nov. 2023, doi: 10.1016/j.egyr.2023.06.022.

[7] B. Shao, Q. Xiao, L. Xiong, L. Wang, Y. Yang, Z. Chen, F. Blaabjerg, and J. M. Guerrero, "Power coupling analysis and improved decoupling control for the VSC connected to a weak AC grid," *Int. J. Electr. Power Energy Syst.*, vol. 145, Feb. 2023, Art. no. 108645, doi: 10.1016/j.ijepes.2022.108645.

[8] X. Mou, D. T. Gladwin, R. Zhao, and H. Sun, "Survey on magnetic resonant coupling wireless power transfer technology for electric vehicle charging," *IET Power Electron.*, vol. 12, no. 12, pp. 3005–3020, Oct. 16, 2019, doi: 10.1049/iet-pel.2019.0529.

[9] K. Aditya and S. S. Williamson, "Design guidelines to avoid bifurcation in a series–series compensated inductive power transfer system," *IEEE Trans. Ind. Electron.*, vol. 66, no. 5, pp. 3973–3982, May 2019, doi: 10.1109/TIE.2018.2851953.

[10] M. Venkatesan, N. Rajamanickam, P. Vishnuram, M. Bajaj, V. Blazek, L. Prokop, and S. Misak, "A review of compensation topologies and control techniques of bidirectional wireless power transfer systems for electric vehicle applications," *Energies*, vol. 15, no. 20, p. 7816, Oct. 01, 2022, doi: 10.3390/en15207816.

[11] M. Kwon, S. Jung, and S. Choi, "A high efficiency bi-directional EV charger with seamless mode transfer for V2G and V2H application," in *Proc. IEEE Energy Convers. Congr. Exposit. (ECCE)*, Sep. 2015, pp. 5394–5399, doi: 10.1109/ECCE.2015.7310418.

[12] M. Venkatesan, R. Narayanamoorthi, K. M. AboRas, and A. Emara, "Efficient bidirectional wireless power transfer system control using dual phase shift PWM technique for electric vehicle applications," *IEEE Access*, vol. 12, pp. 27739–27755, 2024, doi: 10.1109/ACCESS.2024.3367437.
[13] R. K. Yakala, D. Nayak, and S. Pramanick, "Simultaneous output voltage regulation and efficiency enhancement of BWPT systems under lateral misalignment through vehicle side control," in *Proc. IEEE Int. Conf. Power Electron., Smart Grid, Renew. Energy (PESGRE)*, Trivandrum, India, Dec. 2023, pp. 1–6, doi: 10.1109/pesgre58662.2023.10404802.
[14] Z. Fang, J. Wang, J. Liang, Y. Yan, D. Pi, H. Zhang, and G. Yin, "Authority allocation strategy for shared steering control considering human-machine mutual trust level," *IEEE Trans. Intell. Vehicles*, vol. 9, no. 1, pp. 2002–2015, Jan. 2024, doi: 10.1109/tiv.2023.3300152.
[15] Y. Shen, D. Liu, W. Liang, and X. Zhang, "Current reconstruction of three-phase voltage source inverters considering current ripple," *IEEE Trans. Transport Electrific.*, vol. 9, no. 1, pp. 1416–1427, Mar. 2023, doi: 10.1109/TTE.2022.3199431.
[16] H. Wang, Z. Xu, X. Ge, Y. Liao, Y. Yang, Y. Zhang, B. Yao, and Y. Chai, "A junction temperature monitoring method for IGBT modules based on turn-off voltage with convolutional neural networks," *IEEE Trans. Power Electron.*, vol. 38, no. 8, pp. 10313–10328, Aug. 2023, doi: 10.1109/TPEL.2023.3278675.
[17] Y. Lei, C. Yanrong, T. Hai, G. Ren, and W. Wenhuan, "DGNet: An adaptive lightweight defect detection model for new energy vehicle battery current collector," *IEEE Sensors J.*, vol. 23, no. 23, pp. 29815–29830, Dec. 2023, doi: 10.1109/jsen.2023.3324441.
[18] T. Tan, K. Chen, Y. Jiang, Q. Lin, L. Yuan, and Z. Zhao, "A bidirectional wireless power transfer system control strategy independent of real-time wireless communication," *IEEE Trans. Ind. Appl.*, vol. 56, no. 2, pp. 1587–1598, Mar. 2020, doi: 10.1109/TIA.2019.2961311.
[19] S. Jia, C. Chen, S. Duan, and Z. Chao, "Dual-side asymmetrical voltage-cancelation control for bidirectional inductive power transfer systems," *IEEE Trans. Ind. Electron.*, vol. 68, no. 9, pp. 8061–8071, Sep. 2021.
[20] L. Zheng, J. Zhang, Z. Bie, D. Wang, and C. Zhu, "A bidirectional wireless power transfer system for spacecraft docking mechanism," *IEEE 2nd Int. Conf. Electron. Technol., Commun. Inf. (ICETCI)*, pp. 275–280, 2022, doi: 10.1109/ICETCI55101.2022.9832382.
[21] D. Wu, R. Mai, W. Zhou, Y. Liu, F. Peng, S. Zhao, and Q. Zhou, "An improved pulse density modulator in inductive power transfer system," *IEEE Trans. Power Electron.*, vol. 37, no. 10, pp. 12805–12813, Oct. 2022, doi: 10.1109/TPEL.2021.3135281.
[22] H. Li, K. Wang, J. Fang, and Y. Tang, "Pulse density modulated ZVS full-bridge converters for wireless power transfer systems," *IEEE Trans. Power Electron.*, vol. 34, no. 1, pp. 369–377, Jan. 2019, doi: 10.1109/TPEL.2018.2812213.
[23] R. Dai, R. Mai, and W. Zhou, "A pulse density modulation based receiver reactance identification method for wireless power transfer system," *IEEE Trans. Power Electron.*, vol. 37, no. 9, pp. 11394–11405, Sep. 2022, doi: 10.1109/TPEL.2022.3167265.
[24] V. Yenil and S. Cetin, "An improved pulse density modulation control for secondary side controlled wireless power transfer system using LCC-S compensation," *IEEE Trans. Ind. Electron.*, vol. 69, no. 12, pp. 12762–12772, Dec. 2022, doi: 10.1109/TIE.2021.3134059.
[25] A. A. S. Mohamed, A. Berzoy, F. G. N. de Almeida, and O. Mohammed, "Modeling and assessment analysis of various compensation topologies in bidirectional IWPT system for EV applications," *IEEE Trans. Ind. Appl.*, vol. 53, no. 5, pp. 4973–4984, Sep. 2017, doi: 10.1109/TIA.2017.2700281.
[26] D. C. Pandey, P. K. Behera, and M. Pattnaik, "Steady-state analysis of dual active bridge converter with single phase shift and dual phase shift modulation," in *Proc. IEEE Int. Students' Conf. Electr., Electron. Comput. Sci. (SCEECS)*, Bhopal, India, Feb. 2023, pp. 1–6, doi: 10.1109/SCEECS57921.2023.10062987.
[27] H. Naseem and J. Seok, "Triple-phase shift power-level controller (TPSPC) for single-phase dual active bridge (DAB) DC/DC converter," in *Proc. IEEE Energy Convers. Congr. Expo.*, 2022, pp. 1–5, doi: 10.1109/ECCE50734.2022.9947623.
[28] V. Esteve, E. Sanchis-Kilders, J. Jordan, E. J. Dede, C. Cases, E. Maset, J. B. Ejea, and A. Ferreres, "Improving the efficiency of IGBT series-resonant inverters using pulse density modulation," *IEEE Trans. Ind. Electron.*, vol. 58, no. 3, pp. 979–987, Mar. 2011, doi: 10.1109/TIE.2010.2049706.

MURUGAN VENKATESAN received the B.E. degree in electrical and electronics engineering from the Dhanalakshmi College of Engineering, Chennai, and the M.Tech. degree in power electronics and drives from the Arunai College of Engineering and Technology, Tiruvannamalai. He is a Research Scholar with the Department of EEE, SRM Institute of Science and Technology. His research interests include bidirectional wireless power transfer and electric vehicle charging. He is a Lifetime Member of MISTE.

R. NARAYANAMOORTHI received the bachelor's degree in electrical engineering and the master's degree in control and instrumentation from Anna University, India, in 2009 and 2011, respectively, and the Ph.D. degree from the SRM Institute of Science and Technology, India, in 2019. He is an Associate Professor with the Department of Electrical and Electronics Engineering, SRM Institute of Science and Technology. His research interests include wireless power transfer, electric vehicles, power electronics, artificial intelligence and machine learning in renewable energy systems, and embedded systems for smart sensors.

AHMED EMARA was born in Alexandria, Egypt, in 1974. He received the B.S. degree in communication engineering and electro physics and the M.S. and Ph.D. degrees in engineering physics from the Faculty of Engineering, Alexandria University, Egypt, in 1996, 2003, and 2008, respectively. He is currently an Assistant Professor with the College of Engineering, University of Business and Technology, Jeddah, Saudi Arabia. His research interests include semiconductors, optical devices, and optoelectronics.

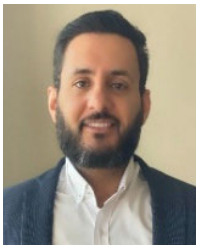

YAZEED YASIN GHADI received the Ph.D. degree in electrical and computer engineering from Queensland University. He was a Postdoctoral Researcher with Queensland University, before joining Al Ain University. He is currently an Assistant Professor of software engineering with Al Ain University. He has published more than 25 peer-reviewed journals and conference papers and holds three pending patents. His current research interests include developing novel electro-acoustic-optic neural interfaces for large-scale high-resolution electrophysiology and distributed optogenetic stimulation. He was a recipient of several awards. His dissertation on developing novel hybrid plasmonic photonic on-chip biochemical sensors received the Sigma Xi Best Ph.D. Thesis Award.